Cellular and Molecular Life Sciences (2022) 79:228
https://doi.org/10.1007/s00018-022-04248-8

ORIGINAL ARTICLE

AUF1 protects against ferroptosis to alleviate sepsis-induced acute lung injury by regulating NRF2 and ATF3

Yichun Wang[1] · Diyu Chen[2] · Han Xie[3] · Mingwang Jia[1] · Xiaofang Sun[3] · Fang Peng[1] · Feifei Guo[1] · Daolin Tang[4]

Received: 17 August 2021 / Revised: 10 March 2022 / Accepted: 16 March 2022 / Published online: 7 April 2022

Abstract

Background The AU-rich element (ARE)-binding factor 1 (AUF1) acts as a switch for septic shock, although its underlying mechanisms remain largely unknown. In this study, we examined the biological significance and potential molecular mechanism of AUF1 in regulating ferroptosis in sepsis-induced acute lung injury (ALI).

Methods Alveolar epithelial cells (AECs) challenged with ferroptosis-inducing compounds and cecum ligation and puncture (CLP)-induced ALI were used as the in vitro and in vivo model, respectively. The stability of AUF1 and its degradation by ubiquitin–proteasome pathway were examined by cycloheximide chase analysis and co-immunoprecipitation assay. The regulation of AUF1 on nuclear factor E2-related factor 2 (NRF2) and activation transcription factor 3 (ATF3) was explored by RNA immunoprecipitation (RIP), RNA pull-down, and mRNA stability assays. Functionally, the effects of altering AUF1, NRF2 or ATF3 on ferroptosis in AECs or ALI mice were evaluated by measuring cell viability, lipid peroxidation, iron accumulation, and total glutathione level.

Results AUF1 was down-regulated in AECs challenged with ferroptosis-inducing compounds, both on mRNA and protein levels. The E3 ubiquitin ligase FBXW7 was responsible for protein degradation of AUF1 during ferroptosis. By up-regulating NRF2 and down-regulating ATF3, AUF1 antagonized ferroptosis in AECs in vitro. In the CLP-induced ALI model, the survival rate of AUF1 knockout mice was significantly reduced and the lung injuries were aggravated, which were related to the enhancement of lung ferroptosis.

Conclusions FBXW7 mediates the ubiquitination and degradation of AUF1 in ferroptosis. AUF1 antagonizes ferroptosis by regulating NRF2 and ATF3 oppositely. Activating AUF1 pathway may be beneficial to the treatment of sepsis-induced ALI.

Keywords Sepsis-induced ALI · Ferroptosis · Ubiquitination · FBXW7 · AUF1 · NRF2 · ATF3

Yichun Wang and Diyu Chen co-first authors.

✉ Yichun Wang
wangyichun2005@sina.com

✉ Daolin Tang
daolin.tang@utsouthwestern.edu

[1] Department of Critical Care Medicine, The Third Affiliated Hospital of Guangzhou Medical University, No.63, Duobao Road, Liwan District, Guangdong 510150, Guangzhou, People's Republic of China

[2] Department of Obstetrics and Gynecology, Key Laboratory for Major Obstetric Diseases of Guangdong Province, The Third Affiliated Hospital of Guangzhou Medical University, Guangdong 510150, Guangzhou, People's Republic of China

[3] Key Laboratory of Reproduction and Genetics of Guangdong Higher Education Institutes, The Third Affiliated Hospital of Guangzhou Medical University, Guangdong 510150, Guangzhou, People's Republic of China

[4] Department of Surgery, UT Southwestern Medical Center, Dallas, TX 75390, USA

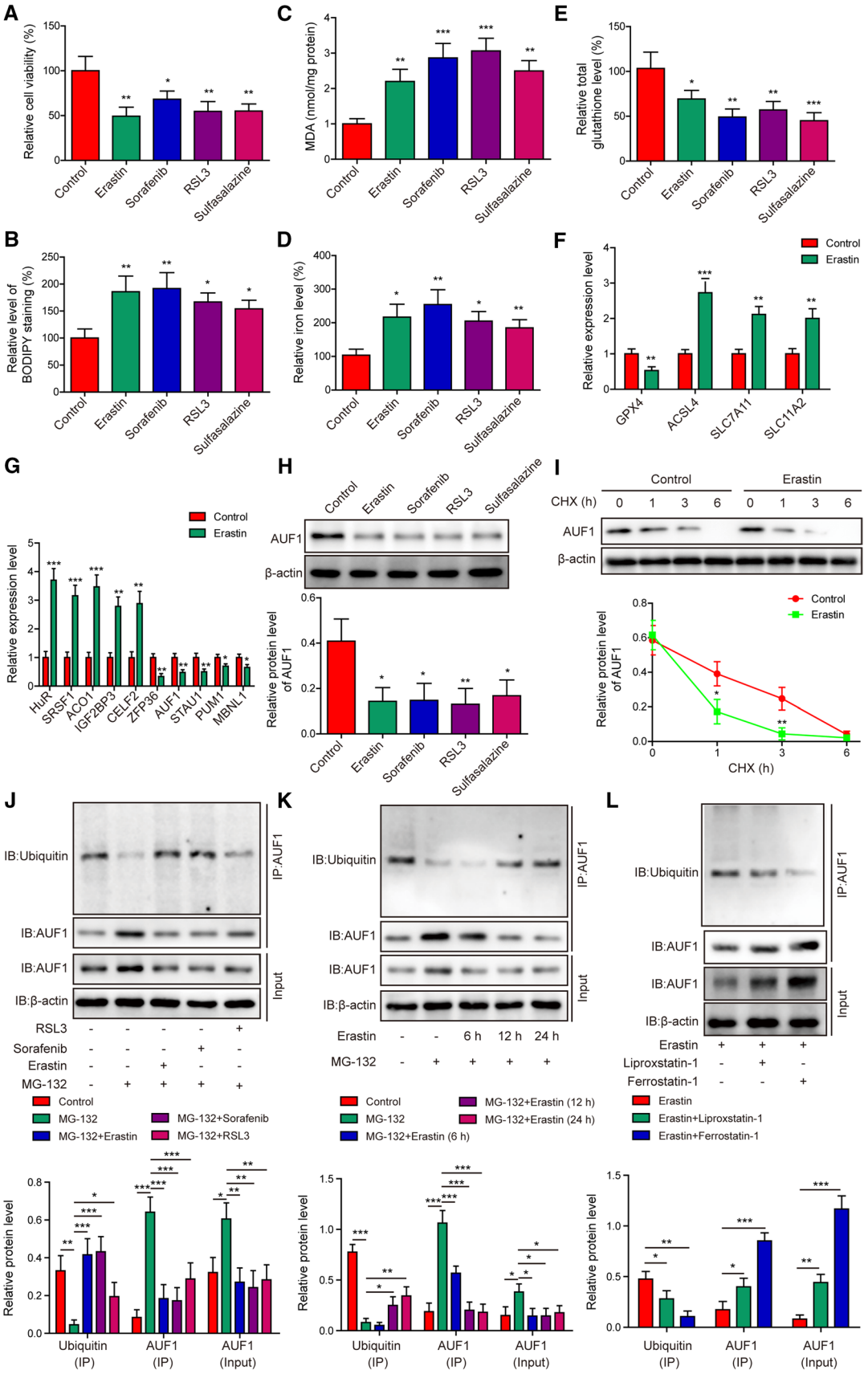
A
Relative cell viability (%)
Control
Erastin
Sorafenib
RSL3
Sulfasalazine
C
MDA (nmol/mg protein)
E
Relative total glutathione level (%)
B
Relative level of BODIPY staining (%)
D
Relative iron level (%)
F
Relative expression level
Control
Erastin
GPX4
ACSL4
SLC7A11
SLC11A2
G
HuR
SRSF1
ACO1
IGF2BP3
CELF2
ZFP36
AUF1
STAU1
PUM1
MBNL1
H
AUF1
β-actin
Relative protein level of AUF1
I
CHX (h)
0 1 3 6 0 1 3 6
CHX (h)
J
IB:Ubiquitin
IB:AUF1
IB:β-actin
IP:AUF1
Input
RSL3
Sorafenib
Erastin
MG-132
Control
MG-132
MG-132+Erastin
MG-132+Sorafenib
MG-132+RSL3
Relative protein level
Ubiquitin (IP)
AUF1 (IP)
AUF1 (Input)
K
Erastin - - 6 h 12 h 24 h
MG-132 - + + + +
MG-132+Erastin (12 h)
MG-132+Erastin (24 h)
MG-132+Erastin (6 h)
L
Liproxstatin-1
Ferrostatin-1
Erastin+Liproxstatin-1
Erastin+Ferrostatin-1

◂**Fig. 1** Ubiquitin–proteasome pathway mediates AUF1 degradation in AECs during ferroptosis. AECs were treated with Erastin (5 μM), Sorafenib (10 μM), RSL3 (10 μM), or Sulfasalazine (20 μM) for 12 h. Ferroptosis was assessed by measuring cell viability using MTT assay (**A**), BODIPY staining (**B**), intracellular MDA (**C**), iron (**D**), and total glutathione **E** levels. **F** The expression levels of ferroptosis-related markers GPX4, ACSL4, SLC7A11, and SLC11A2 were examined by RT-PCR in control or Erastin-treated AECs. **G** The expression levels of indicated RBPs were examined by RT-PCR in control or Erastin-treated AECs. **H** The protein level of AUF1 was examined by western blot in AECs stressed with Erastin, Sorafenib, RSL3, or Sulfasalzine. **I** The degradation of AUF1 protein was examined by CHX chase assay, where AECs were treated with CHX (5 μg/mL) for indicated time periods. The ubiquitination of AUF1 was examined by Co-IP using anti-AUF1 antibody, after proteasome signaling of AECs was blocked with MG-132 (25 μM) for 2 h, then AECs were treated with Erastin (5 μM), Sorafenib (10 μM), or RSL3 (10 μM) for 12 h (**J**); after proteasome signaling of AECs was blocked with MG-132 (25 μM) for 2 h, then AECs were treated with Erastin (5 μM) for indicated time periods (K); after AECs were treated with Erastin (5 μM), without or with Liproxastatin-1 (25 nM) or Ferrostatin-1 (100 nM) for 12 h (**L**). $^{*}P<0.05$, $^{**}P<0.01$ and $^{***}P<0.001$

Introduction

Sepsis is a life-threatening systemic condition and a leading cause of acute lung injury (ALI), including its more severe and advanced form: acute respiratory distress syndrome (ARDS). ALI/ARDS is strongly related to the development of multiple organ dysfunction syndrome and the increased mortality of sepsis patients [1]. The pathophysiological features of ALI include diffuse damage to alveolar epithelial cells (AECs) and microvascular endothelial cells, pulmonary edema, and excessive neutrophil-derived inflammation [2, 3]. Apoptosis is the major mechanism responsible for AEC damage in ALI, yet recent studies suggest that ferroptosis also contributes to AEC death in ALI induced by various stresses, such as radiation, ischemia/reperfusion, lipopolysaccharides and oleic acid [4–7]. However, there is limited information on the potential contribution of ferroptosis to sepsis-induced ALI.

Ferroptosis is a form of iron-dependent and apoptosis-independent cell death [8, 9]. Many compounds have been identified to induce ferroptosis, such as erastin, ras-selective lethal small molecule 3 (RSL3), RSL5, sorafenib, buthioninesulfoximine, acetaminophen, aretesunate, and sulfasalazine [9]. At the cellular level, ferroptosis is characterized by reduced cell viability, increased intracellular iron level and lipid peroxidation, and decreased antioxidant capacities (such as glutathione depletion) [8]. Several signal transduction pathways that regulate ferroptosis by targeting iron metabolism and lipid peroxidation have been revealed, which lead to the identification of multiple ferroptosis regulators. For example, voltage-dependent anion channel 2/3 (VDAC2/3), Ras, NOX, p53, cysteinyl-tRNA synthetase (CARS), acyl-CoA synthetase long-chain family member 4 (ACSL4), solute carrier family 11 member 2 (SLC11A2), and activation transcription factor 3 (ATF3) are positive regulators of ferroptosis, whereas glutathione peroxidase 4 (GPX4), system X_c^- (a heterodimer composed of SLC7A11 and SLC3A2), and nuclear factor E2-related factor 2 (NRF2) are negative regulators of ferroptosis [8–10].

To understand the link between ferroptosis and sepsis-induced ALI, we focused on the AU-rich element (ARE)-binding factor 1 (AUF1, also known as heterogeneous nuclear ribonucleoprotein D [HNRNPD]). AUF1 is an mRNA-binding protein (mRBP), which is a crucial switch to turn off the inflammatory response and to alleviate sepsis-related symptoms [11]. Furthermore, AUF1 could impact the mRNA stability of two ferroptosis regulators NRF2 and ATF3 [12, 13]. In this study, we combined AECs cultured in vitro and a mouse model of sepsis induced by cecum ligation and puncture (CLP), and examined the alteration of AUF1 during ferroptosis, the molecular mechanism leading to this change, the biological significance of AUF1 in ferroptosis and sepsis-induced ALI, as well as the signaling pathways responsible for the role of AUF1. We provided the first evidence that by positively regulating NRF2 and negatively modulating ATF3, AUF1 is a critical negative regulator of ferroptosis. Consequently, the knockdown of AUF1 aggravates sepsis-induced ALI damages and deteriorates the overall survival of mice in a ferroptosis-dependent manner. We also demonstrate the E3 ligase FBXW7 is responsible for protein degradation of AUF1 during ferroptosis.

Materials and methods

Cell culture and reagents

The human primary pulmonary AECs were purchased from Cell Biologics (Chicago, IL, USA) and cultured in Complete Human Epithelium Cell Medium (Cell Biologics). Cells between passages 2 and 4 were used in the study. Erastin (E7242), Sorafenib (S7397), Sulfasalazine (S1576), RSL3 (S8155), Actinomycin D (S8964), Ferrostatin-1 (S7243), and Liproxstatin-1 (S7699) were all obtained from Selleck Chemicals (Houston, TX, USA). Cycloheximide (CHX, C4859) and MG-132 (M7449) were purchased from Sigma (St. Louis, MO, USA).

3-(4, 5-dimethylthiazolyl-2)-2, 5-diphenyltetrazolium bromide (MTT) assay

Cells were seeded in 96-well plates at a density of 2×10^4 cells/mL. Then 20 μL of MTT solution (5 mg/mL

in PBS, Sigma) was added to each well and the plates were incubated at 37 °C for a further 3 h. The medium was then discarded and 100 µL of dimethyl sulfoxide (DMSO, Sigma) was added to each well and incubated for 2 h in the dark at room temperature. DMSO dissolved the formazan crystals and created a purple color. Finally, the optical density (OD, proportional to the number of live cells) was assessed with a Microplate Reader Bio-Rad 550 at 570 nm. The percentage (%) of cell viability was calculated as $(OD_{experiment}\text{-}OD_{blank})/(OD_{control}\text{-}OD_{blank}) \times 100\%$.

Lipid peroxidation, iron, and GSH detection

The malondialdehyde (MDA) concentration in cell lysates was assessed using a Lipid Peroxidation Assay Kit (ab118970, Abcam) according to the manufacturer's instruction. Also, the relative iron concentration and total glutathione level in cell lysates were assessed using an Iron Assay Kit (ab83366, Abcam) and a Glutathione Assay Kit (CS0260, Sigma), respectively, according to the manufacturer's instructions. Myeloperoxidase (MPO) Activity Assay Kit (ab105136, Abcam) was used to test MPO activity in lung tissues.

BODIPY staining

The staining of lipid peroxides in cells was performed as described previously [14] using BODIPY 581/591 C11 Probe (D3861, Thermo Fisher Scientific, Waltman, MA, USA). The level of BODIPY staining was detected by flow cytometry using FACSCalibur (BD Biosciences, San Jose, CA, USA).

Generation and transduction of lentivirus

Lentiviral vectors overexpressing AUF1, ATF3, shRNA targeting FBXW7 (shFBXW7), shNRF2, or control shRNA (shNC) were constructed and produced by GeneCopoeia (Guangzhou, China). To generate lentivirus, lentiviral and packaging vectors were co-transfected into 293T cells. At 48 h after the transfection, the supernatant containing lentivirus was collected and concentrated using Lenti-Pac Lentivirus Concentration Solution (GeneCopoeia) according to the manufacturer's instruction. After determining the titer, lentivirus was transduced into target cells at a multiplicity of infection (MOI) of 50 in the presence of polybrene (8 µg/mL, Sigma) overnight.

RNA extraction and real-time PCR (RT-PCR)

Total RNA was extracted from cells or mouse lung tissues using Trizol (Invitrogen, Carlsbad, CA, USA) and reversely transcribed into cDNA using SuperScript III Reverse Transcriptase (Invitrogen). RT-PCR was performed with SYBR Green Master Mix (Applied Biosystems, Foster City, CA, USA) on the ABI PRISM 7900 Sequence Detection System (Applied Biosystems). Primer sequences used for RT-PCR were purchased from Sangon Biotech (Shanghai). The gene relative expression was calculated using the $2^{-\Delta\Delta Ct}$ method and presented as a ratio to that of β-actin (internal control).

Western blotting

The cultured cells and mouse lung tissues were lysed with RIPA buffer (Thermo Fisher Scientific) and the protein concentration was measured using the BCA Protein Assay Kit (Thermo Fisher Scientific). Then 20 µg of total protein from each sample was separated on 10% SDS-PAGE and electro-transferred to polyvinylidence difluoride (PVDF) membrane. After blocking with 5% non-fat milk at room temperature for 1 h, the membrane was incubated with primary antibodies (all from Cell Signaling Technology, Danvers, MA, USA, unless otherwise indicated) at 4 °C overnight: anti-AUF1 (#12382, 1:1000), anti-ubiquitin (#3936, 1:1000), anti-FBXW7 (ab109617, 1:1500, Abcam), anti-GPX4 (ab125066, 1:2000, Abcam), anti-ACSL4 (ab155282, 1:1500, Abcam), anti-SLC7A11 (, 1:2000), anti-SLC11A2 (ab55735, 1:2000, Abcam), anti-NRF2 (#12721, 1:1000), anti-heme oxygenase 1 (HO-1, #70081, 1:1000), anti-ATF3 (#18665, 1:2000), and anti-β-actin (#3700, 1:3000). After three washes, the membrane was incubated with horseradish peroxidase-conjugated secondary antibodies (1:2000). The bands were detected with ECL substrate (Thermo Fisher Scientific) and normalized to β-actin.

Co-immunoprecipitation (Co-IP)

Cultured cells were lysed in 25 mM Tris–HCl (pH 7.4) containing 150 mM NaCl, 1 mM EDTA, 1% NP-40, 5% glycerol, and protease/phosphatase inhibitor cocktail (Cell Signaling Technology). IP was performed using Pierce Co-Immunoprecipitation Kit (Thermo Fisher Scientific) together with either anti-ubiquitin antibody (ab140601, Abcam), anti-AUF1 (#12382, Cell Signaling Technology) or anti-FBXW7 (ab109617, Abcam) antibody. The IP complex was analyzed by western blot.

RNA immunoprecipitation (RIP) assay

The RIP experiment was performed using the Magna RIP RNA-Binding Protein Immunoprecipitation Kit (17-700, Millipore) following the manufacturer's instruction. After incubation of the cell lysate with the magnetic beads conjugated to anti-AUF1 (#12382, Cell Signaling Technology)

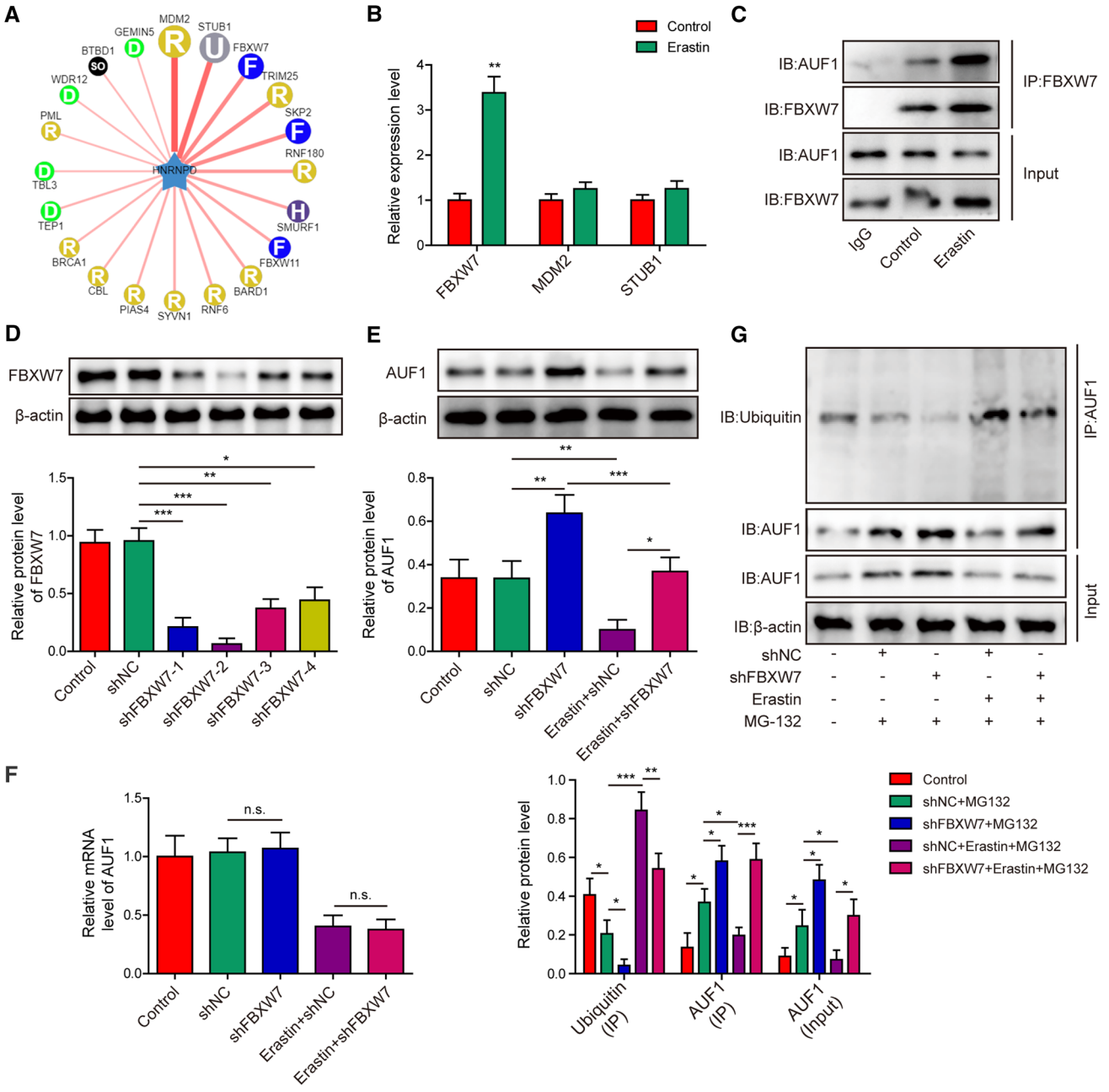

Fig. 2 E3 ubiquitin ligase FBXW7 is responsible for the degradation of AUF1 during ferroptosis. **A** Network indicated potential E3 ubiquitin ligases for AUF1 (HNRNPD) as predicted using UbiBrowser database (http://ubibrowser.ncpsb.org.cn/ubibrowser/). Thicker lines indicated higher likelihood ratio. **B** The expression levels of FBXW7, MDM2 and STUB1 were compared by RT-PCR between control and Erastin-treated AECs (Erastin at 5 μM for 12 h). **C** The interaction between FBXW7 and AUF1 was examined by Co-IP using anti-FBXW7 antibody in control and Erastin-treated AECs (Erastin at 5 μM for 12 h). IgG antibody was used as the negative control. **D** Lentivirus expressing either control shRNA (shNC) or four distinct shRNA targeting FBXW7 (shFBXW7-1 to -4) was transduced into AECs for 48 h. Non-transduced AECs were used as control. The protein level of FBXW7 was examined by western blot. **E**, **F** The expression of AUF1 was determined by western blot **E** and RT-PCR **F** in control, shNC- or shFBXW7-transfeted AECs challenged with or without Erastin (5 μM for 12 h). **G** The ubiquitination of AUF1 was examined by Co-IP using anti-AUF1 antibody in control, shNC- or shFBXW7-transfeted AECs challenged with or without Erastin (5 μM for 12 h) upon MG-132 pre-treatment (25 μM for 2 h). $^{*}P<0.05$, $^{**}P<0.01$ and $^{***}P<0.001$. *n.s.* not significant

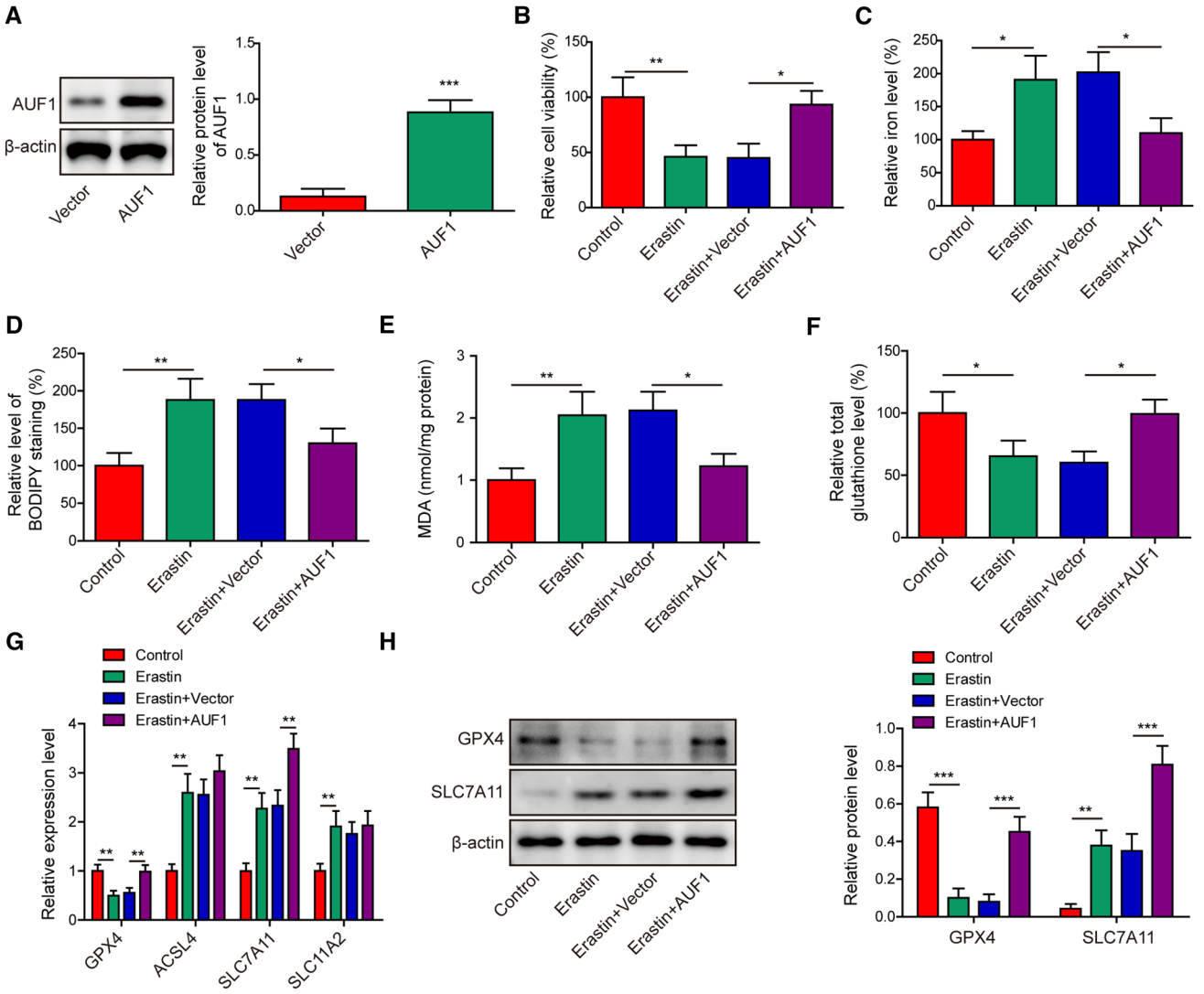

Fig. 3 AUF1 antagonizes Erastin-induced ferroptosis. **A** AUF1-overepressing and control vector lentiviruses were transduced into AECs for 48 h. The protein level of AUF1 was determined by western blot. **B**–**F** Ferroptosis was assessed by measuring cell viability using MTT assay (**B**), intracellular iron (**C**), BODIPY staining (**D**), MDA (**E**), and total glutathione **F** levels in vector or AUF1 overexpressed AECs challenged with or without Erastin (5 μM for 12 h). **G** The expression levels of GPX4, ACSL4, SLC7A11, and SLC11A2 were examined by RT-PCR in vector or AUF1 overexpressed AECs challenged with or without Erastin (5 μM for 12 h). **H** The expression levels of GPX4 and SLC7A11 were examined by western blot in vector or AUF1 overexpressed AECs challenged with or without Erastin (5 μM for 12 h). $^{*}P<0.05$, $^{**}P<0.01$ and $^{***}P<0.001$

or normal rabbit IgG (Cell Signaling Technology) antibody, the NRF2 or ATF3 expression in co-precipitated RNA was detected by qPCR. Target RNA detected from total RNA was used as the input control. The RNA binding with IgG was used as the negative control.

RNA pull-down assay

Biotin-labeled RNA transcripts were synthesized by in vitro transcription with T7 RNA polymerase in the presence of biotin-UTP. PCR fragments corresponding to 5'-UTR, coding sequence (CDS) and 3'-UTR of human NRF2 or ATF3 gene were amplified with forward primers containing T7 RNA polymerase promoter sequences and reverse primers containing T3 RNA polymerase promoter sequences. Purified PCR products were used as DNA template for in vitro transcription. Whole cell lysates (300–500 μg per sample) were incubated with purified biotinylated RNA probes (~ 10 pmol) for 25 min at 30 °C. RNA–protein complexes were further isolated by streptavidin sepharose high performance beads (GE Healthcare). The recruited proteins were detected by western blot.

Measurement of mRNA stability

To measure mRNA stability, cells were treated with Actinomycin D (2.5 μg/mL) for indicated time periods. Target mRNAs were then detected by RT-PCR analysis.

Establishment of CLP-induced sepsis model

AUF1 knockout (KO) and wildtype (WT) mice (n = 20 per group) were purchased from SJA Laboratory Animal Co, Ltd (Changsha, Hunan, China). All animal protocols were reviewed and approved by the Institutional Animal Care and Use Committee of Guangzhou Medical University (Guangzhou, Guangdong, China). CLP procedure was performed as described previously [15]. Briefly, under anesthesia, an incision of 1 cm in length was made along the midline and the cecum was exposed. Then the cecum was ligated with a 3/0 silk suture in the middle and punctured twice using a 21-gauge needle close to the distal end. A small amount of stool was extruded. The cecum was repositioned and the abdomen was closed. For sham group, mice received the same surgical procedure but not ligation and puncture. Immediately after the surgery, all mice received a subcutaneous injection of 1 mL 37 °C normal saline for fluid resuscitation. For ferrostatin-1 treatment, 1 mg/kg ferrostatin-1 was intraperitoneally injected into mice for two consecutive days before CLP operation. Mice survival was monitored daily and lung tissues, serum, and bronchoalveolar lavage fluid (BALF) were collected after 24 h for further analyses.

Histopathology analysis

The mouse lung tissues were fixed in 10% neutral formalin, embedded in paraffin, and processed into serial sections of 4 μm in thickness. Hematoxylin and eosin (HE) staining was performed using HE staining Kit (Vector Labs, Burlingame, CA, USA) according to the manufacturer's instruction. The severity of lung injury was scored as described previously [16]. What's more, the injury of lung tissues was measured by the TUNEL assay using In Situ Cell Death Detection Kit (Roche, Basel, Switzerland) following the manufacturer's instruction.

Lung wet-to-dry (W/D) weight ratio

The lung tissues were excised, washed in PBS, gently dried using blotting paper, and weighed. The tissues were then dried at 60 °C for 72 h and reweighed.

Collection and procession of BALF and serum

BALF was collected as described previously [17] and centrifuged at 400 × *g* for 10 min to separate the supernatant from cells. The total cell number from BALF was counted using a hemocytometer. Blood was collected 24 h after operation and serum was separated upon centrifugation at 2000 × *g* for 10 min. The concentrations of TNF-α, IL-1β, and IL-6 in serum and BALF supernatant were measured using ELISA kits for the corresponding cytokines. All the ELISA kits are from Abcam, except IL-6 ELISA Kit (R&D System, Minneapolis, MN, USA).

Statistical analysis

All data were analyzed by GraphPad Prism 6.0 and presented as mean ± standard deviation (SD) from three independent experiments (for in vitro assays) or from multiple mice within each group (for in vivo experiments). Differences between experimental groups were assessed by the Student's *t* test or one-way analysis of variance (ANOVA) followed by Tukey's post hoc test. The overall survival curve was mapped with Kaplan–Meier method and analyzed using the log rank test. A *P* value of less than 0.05 was considered statistically significant.

Results

Ubiquitin–proteasome pathway mediates AUF1 degradation in AECs during ferroptosis

To understand the pathogenic mechanism underlying ferroptosis in acute lung injury, we treated AECs with four distinct ferroptosis-inducing compounds including Erastin, Sorafenib, RSL3, and Sulfasalazine [9]. As shown in Fig. 1A, all four compounds significantly reduced cell viability, when compared to those treated with vehicle control. Correspondingly, staining with BODIPY (for measuring lipid peroxides) (Fig. 1B), the intracellular levels of MDA (an end-product of lipid peroxides) (Fig. 1C) and iron (Fig. 1D) were significantly increased, while the level of total glutathione was decreased (Fig. 1E) in stressed cells. At the molecular level, the mRNA level of GPX4 was decreased, whereas the mRNA levels of ACSL4, SLC7A11, and SLC11A2 were upregulated (Fig. 1F) in AECs following Erastin treatment. These data indicate the successful induction of ferroptosis by these compounds.

To explore the involvement of RBPs in this process, we compared the expression of a panel of RBPs between control and Erastin-treated AECs (Fig. 1G). We found that HuR, SRSF1, ACO1, IGF2BP3 and CELF2 were all significantly up-regulated, while ZFP36, AUF1, STAU1, PUM1, and MBNL1 potently down-regulated by Erastin, suggesting the significance of RBPs in ferroptosis. Next, we focused on AUF1 because all four compounds that induced ferroptosis significantly reduced the protein level of AUF1 in AECs

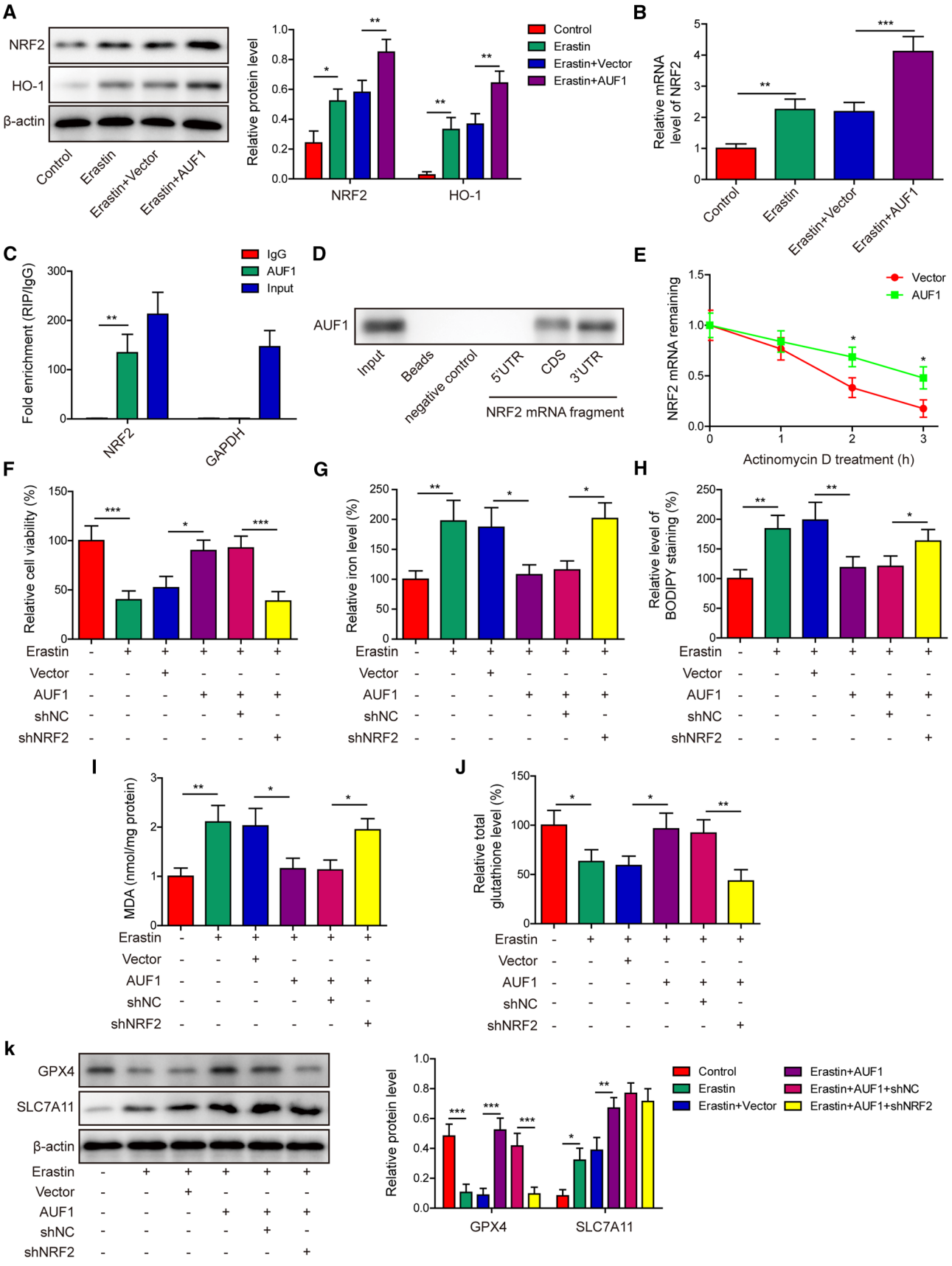
A
NRF2
HO-1
β-actin
Control
Erastin
Erastin+Vector
Erastin+AUF1
Relative protein level
NRF2
HO-1
B
Relative mRNA level of NRF2
C
IgG
AUF1
Input
Fold enrichment (RIP/IgG)
NRF2
GAPDH
D
AUF1
Input
Beads
negative control
5'UTR
CDS
3'UTR
NRF2 mRNA fragment
E
Vector
AUF1
NRF2 mRNA remaining
Actinomycin D treatment (h)
F
Relative cell viability (%)
G
Relative iron level (%)
H
Relative level of BODIPY staining (%)
Erastin
Vector
AUF1
shNC
shNRF2
I
MDA (nmol/mg protein)
J
Relative total glutathione level (%)
k
GPX4
SLC7A11
β-actin
Relative protein level
Erastin+AUF1+shNC
Erastin+AUF1+shNRF2

◂**Fig. 4** AUF1 alleviates ferroptosis by up-regulating NRF2. **A** The expression levels of NRF2 and HO-1 were examined by western blot in vector or AUF1 overexpressed AECs challenged with or without Erastin (5 μM for 12 h). **B** The mRNA level of NRF2 was examined by RT-PCR in vector or AUF1 overexpressed AECs challenged with or without Erastin (5 μM for 12 h). **C** The binding of AUF1 to NRF2 mRNA in AECs was examined by RIP assay using anti-AUF1 antibody. IgG was used as the negative control. **D** The binding of AUF1 to CDS and 3'-UTR of NRF2 mRNA was examined by RNA pull-down assay. **E** The vector or AUF1 overexpressed AECs were treated with Actinomycin D (2.5 μg/mL) for indicated time periods and NRF2 mRNA was determined at indicated time points. **F**–**J** Ferroptosis was assessed by measuring cell viability using MTT assay (**F**), intracellular iron (**G**), BODIPY staining (**H**), MDA (**I**), and total glutathione **J** levels in indicated cells after AUF1 was overexpressed and/or NRF2 was knocked down for 48 h and cells were then challenged with or without Erastin (5 μM for 12 h). **K** The expression levels of GPX4 and SLC7A11 were examined by western blot in indicated cells after AUF1 was overexpressed and/or NRF2 was knocked down for 48 h and cells were then challenged with or without Erastin (5 μM for 12 h). $^{*}P < 0.05$, $^{**}P < 0.01$ and $^{***}P < 0.001$

(Fig. 1H). Since the ubiquitin–proteasome system critically controls the decay of AUF1 protein [18], we then measured the decay of AUF1 protein in control and Erastin-treated cells using the CHX chase analysis. As shown in Fig. 1I, Erastin significantly boosted the degradation of AUF1 protein. Next, we treated AECs with MG-132, a proteasome inhibitor, with or without the ferroptosis-inducing compounds. Compared to control group, MG-132 significantly increased total but reduced ubiquitinated AUF1 protein levels, while the co-treatment of cells with MG-132 and Erastin, Sorafenib, or RSL3 partially or almost completely abolished the inhibition of MG-132 on the ubiquitination of AUF1, and thus reduced total AUF1 protein level (Fig. 1J). The ubiquitination-promoting effect of Erastin on AUF1 was time-dependent (Fig. 1K) and antagonized by ferroptosis inhibitor, Liproxstatin-1 [19] or Ferrostatin-1 [20], as either was sufficient to reduce ubiquitinated AUF1 and elevated total AUF1 protein level (Fig. 1L). Collectively, these data suggested that ferroptosis-inducing compounds significantly reduced AUF1 expression level in AECs via the ubiquitin–proteasome system and this regulation is closely associated with ferroptosis.

E3 ubiquitin ligase FBXW7 is responsible for the degradation of AUF1 during ferroptosis.

To identify the E3 ubiquitin ligases responsible for AUF1 degradation in AECs, we used UbiBrowser (http://ubibrowser.ncpsb.org.cn/ubibrowser/). This bioinformatics analysis showed that MDM2, STUB1, and FBXW7 were the top three E3 ubiquitin ligases that presented the highest likelihood score to interact with AUF1 (HNRNPD, Fig. 2A). Next, we detected the expression of these E3 ubiquitin ligases in Erastin-treated AECs and found that only FBXW7 was significantly up-regulated by Erastin (Fig. 2B), suggesting that FBXW7 might be the E3 ubiquitin ligase for degradation of AUF1. Co-IP analysis showed that AUF1 interacted with FBXW7 in non-treated AECs and this interaction was further boosted in Erastin-treated cells, despite the reduction of total AUF1 protein level (Fig. 2C). To assess the significance of FBXW7 in mediating the degradation of AUF1, we established lentivirus expressing shRNA specifically targeting FBXW7 (shFBXW7). Among the four shFBXW7 lentiviruses tested, #2 presented the best knockdown effect on FBXW7 (Fig. 2D) and thus was used for further experiments. Knockdown of FBXW7 not only boosted the AUF1 protein level in control cells, but abolished Erastin-induced reduction of AUF1 protein (Fig. 2E). In contrast, the knockdown of FBXW7 minimally affected the mRNA level of AUF1, in the absence or the presence of Erastin (Fig. 2F). Consistent with the function of FBXW7 as E3 ubiquitin ligase, shFBXW7 significantly reduced the ubiquitinated AUF1 and thus boosted total AUF1 level in control and Erastin-treated cells (Fig. 2G). Taken together, these data suggest that FBXW7 is the E3 ubiquitin ligase responsible for AUF1 protein degradation in AECs.

AUF1 antagonizes Erastin-induced ferroptosis

The downregulation of AUF1 by ferroptosis-inducing compounds (Fig. 1H) suggested that AUF1 might be functionally important for ferroptosis. To understand the biological significance of AUF1 in ferroptosis, we overexpressed AUF1 in AECs (Fig. 3A). Upon Erastin treatment, the overexpression of AUF1 significantly improved cell viability (Fig. 3B) and intracellular total glutathione level (Fig. 3F), while reduced intracellular iron level (Fig. 3C), the level of BODIPY staining (Fig. 3D), or the intracellular MDA level (Fig. 3E). Among the four ferroptosis-related biomarkers, overexpressing AUF1 rescued Erastin-induced downregulation of GPX4, further up-regulated SLC7A11 at mRNA (Fig. 3G) and protein (Fig. 3H) levels, but minimally impacted the mRNA levels of ACSL4 or SLC11A2 (Fig. 3G). These data indicated that AUF1 played a potent role in inhibiting Erastin-induced ferroptosis.

AUF1 alleviates ferroptosis by up-regulating NRF2

To understand the molecular mechanism underlying AUF1-mediated protection against ferroptosis, we focused on two transcription factors, NRF2 and ATF3. The former can mitigate ferroptosis [21] and the latter can stimulate it [10]. As shown in Fig. 4A, B, both the protein and mRNA levels of NRF2 were significantly increased in Erastin-treated cells, but were further boosted in Erastin + AUF1 cells, suggesting the sufficiency of AUF1 in up-regulating NRF2. Consistently, HO-1, a downstream target of NRF2, presented the same pattern of changes as NRF2 in response to Erastin and/or AUF1 (Fig. 4A). RIP assay showed that AUF1

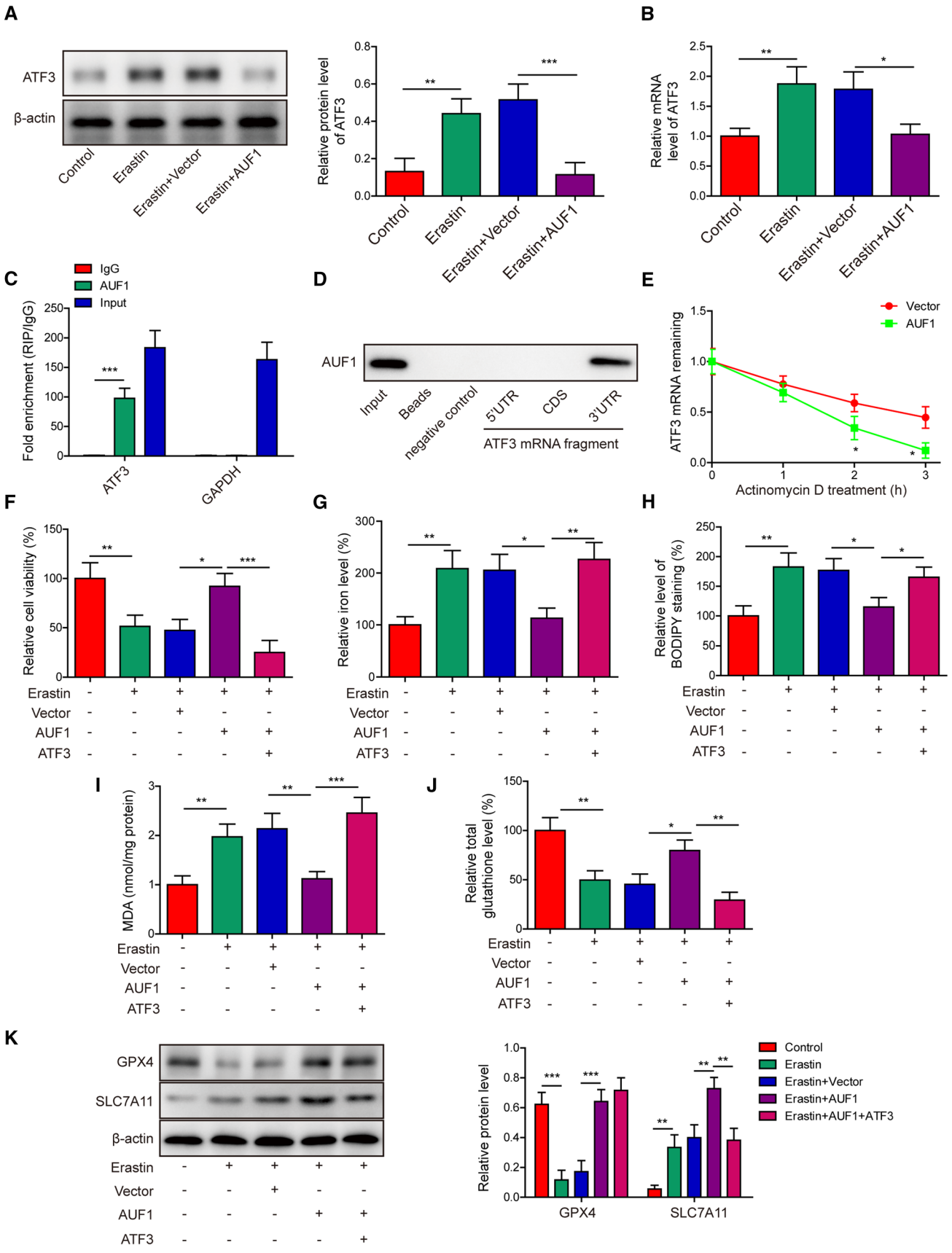
A
ATF3
β-actin
Control
Erastin
Erastin+Vector
Erastin+AUF1
Relative protein level of ATF3
B
Relative mRNA level of ATF3
C
IgG
AUF1
Input
Fold enrichment (RIP/IgG)
ATF3
GAPDH
D
AUF1
Input
Beads
negative control
5'UTR
CDS
3'UTR
ATF3 mRNA fragment
E
Vector
AUF1
ATF3 mRNA remaining
Actinomycin D treatment (h)
F
Relative cell viability (%)
G
Relative iron level (%)
H
Relative level of BODIPY staining (%)
Erastin
Vector
AUF1
ATF3
I
MDA (nmol/mg protein)
J
Relative total glutathione level (%)
K
GPX4
SLC7A11
β-actin
Relative protein level
Control
Erastin
Erastin+Vector
Erastin+AUF1
Erastin+AUF1+ATF3

◂**Fig. 5** AUF1 protects against ferroptosis by down-regulating ATF3. (A-B) The expression levels of ATF3 were examined by western blot **A** and RT-PCR **B** in vector or AUF1 overexpressed AECs challenged with or without Erastin (5 μM for 12 h). **C** The binding of AUF1 to ATF3 mRNA in AECs was examined by RIP assay using anti-AUF1 antibody. IgG was used as the negative control. **D** The binding of AUF1 to 3'-UTR of ATF3 mRNA was examined by RNA pull-down assay. **E** The vector or AUF1 overexpressed AECs were treated with Actinomycin D (2.5 μg/mL) for indicated time periods and ATF3 mRNA was determined at indicated time points. **F**–**J** Ferroptosis was assessed by measuring cell viability using MTT assay (**F**), intracellular iron (**G**), BODIPY staining (**H**), MDA (**I**), and total glutathione **J** levels in indicated cells after AUF1 and ATF3 were overexpressed for 48 h and cells were then challenged with or without Erastin (5 μM for 12 h). **K** The expression levels of GPX4 and SLC7A11 were examined by western blot in indicated cells after AUF1 and ATF3 were overexpressed for 48 h and cells were then challenged with or without Erastin (5 μM for 12 h). *$P<0.05$, **$P<0.01$ and ***$P<0.001$

specifically bound to the mRNA of NRF2, but not that of GAPDH (Fig. 4C). RNA pull-down analysis revealed the binding of AUF1 to CDS and 3'-UTR, but not 5'-UTR of NRF2 mRNA (Fig. 4D). To measure the impact of AUF1 on the mRNA stability of NRF2, we treated AUF1-overexpressing or vector control cells with Actinomycin D and found that NRF2 mRNA was noticeably more stable in AUF1-overexpressing cells (Fig. 4E).

To understand the significance of NRF2 in ferroptosis, we first knocked down endogenous NRF2 level in AECs with lentivirus expressing shNRF2, and exposed cells to vehicle or Liproxstatin-1 (inhibitor of ferroptosis). As shown in Supplementary Fig. S1, when compared to shNC cells, shNRF2 cells presented significantly reduced viability (supplementary Fig. S1A) and intracellular total glutathione level (Supplementary Fig. S1D), but robust increase of intracellular iron level (Supplementary Fig. S1B) and BODIPY staining level (Supplementary Fig. S1C). Applying Liproxstatin-1 partially abolished ferroptosis-promoting effect of shNRF2 (supplementary Fig. S1A–D). Next, we simultaneously expressed AUF1 and knocked down NRF2 in AECs (AUF1 + shNRF2), and used AUF1 + shNC as a negative control. In response to Erastin challenge, AUF1-overexpressing cells (Erastin + AUF1) presented significantly improved cell viability (Fig. 4F) and total glutathione level (Fig. 4J), but reduced intracellular iron level (Fig. 4G), the BODIPY staining level (Fig. 4H), or the intracellular MDA level (Fig. 4I), when compared to Erastin + Vector cells. These anti-ferroptosis effects of AUF1 were mostly abolished in AUF1 + shNFR2 cells (Fig. 4F–J). On the molecular level, compared to AUF1 + shNC cells, we observed the inhibition of GPX4, but no appreciable effect on SLC7A11 expression in AUF1 + shNRF2 cells (Fig. 4K). In collection, these findings suggested that AUF1 directly up-regulated NRF2 by stabilizing its mRNA. In return, NRF2 mediated the anti-ferroptosis function of AUF1 by regulating GPX4 level.

AUF1 protects against ferroptosis by down-regulating ATF3

Next, we investigated the effects of AUF1 on the other transcription factor, ATF3. The protein (Fig. 5A) and mRNA (Fig. 5B) levels of ATF3 were both significantly upregulated in Erastin-treated cells, but the increase in ATF3 expression was completely abolished in Erastin + AUF1 cells. RIP assay showed that AUF1 directly and specifically bound to the mRNA of ATF3 (Fig. 5C) and RNA pull-down identified that the binding was limited to 3'-UTR, but not 5'-UTR or CDS of ATF3 mRNA (Fig. 5D). mRNA stability assay further showed that the overexpression of AUF1 significantly promoted the degradation of ATF3 mRNA (Fig. 5E). When ATF3 was overexpressed in Erastin-challenged AUF1 cells (AUF1 + ATF3), we found that it deteriorated the anti-ferroptosis effects of AUF1 by reducing cell viability (Fig. 5F) and total glutathione level (Fig. 5J), while increasing the iron level (Fig. 5G), BODIPY staining level (Fig. 5H), and MDA level (Fig. 5I). On the molecular level, GPX4 was not altered, but SLC7A11 was reduced in Erastin-treated AUF1 + ATF3 cells, when compared to Erastin-treated AUF1 cells (Fig. 5K). These findings suggested that down-regulating ATF3 and subsequent SLC7A11 also played a role in mediating the anti-ferroptosis function of AUF1.

Ferroptotic damage mediates sepsis-induced ALI in vivo

The findings of in vitro studies suggested that AUF1, by oppositely regulating NRF2 and ATF3, protected AECs from Erastin-induced ferroptosis. To understand whether these findings are relevant in mice involving ferroptosis, we established a sepsis-induced ALI mouse model, which is a disease model involving ferroptosis [22]. We first examined the effect of inhibiting ferroptosis with ferrostatin-1 in alleviating CLP-induced sepsis, with specific focus on the lung injury. As shown in Fig. 6A, ferrostatin-1 had no impact on the survival of sham-operated mice, but improved the survival of CLP mice. Moreover, we observed obvious pulmonary damages in the CLP group, as demonstrated by alveolar epithelium disruption, pulmonary interstitial hyperemia and edema, and massive infiltration of inflammatory cells (Fig. 6B). All these changes were at least partially improved in CLP + ferrostatin-1 mice. Quantitatively, we observed a robust increase in the lung injury score in CLP mice, which was markedly reduced in CLP + ferrostatin-1 mice (Fig. 6C). A similar pattern of changes was also observed in cell death in lung tissues by TUNEL staining (Fig. 6D–E), and the production of pro-inflammatory cytokines such as TNF-α, IL-1β, and IL-6 from the serum (Fig. 6F) and BALF (Fig. 6G), pulmonary edema (Fig. 6H), pulmonary MPO activity (Fig. 6I), total cell number in

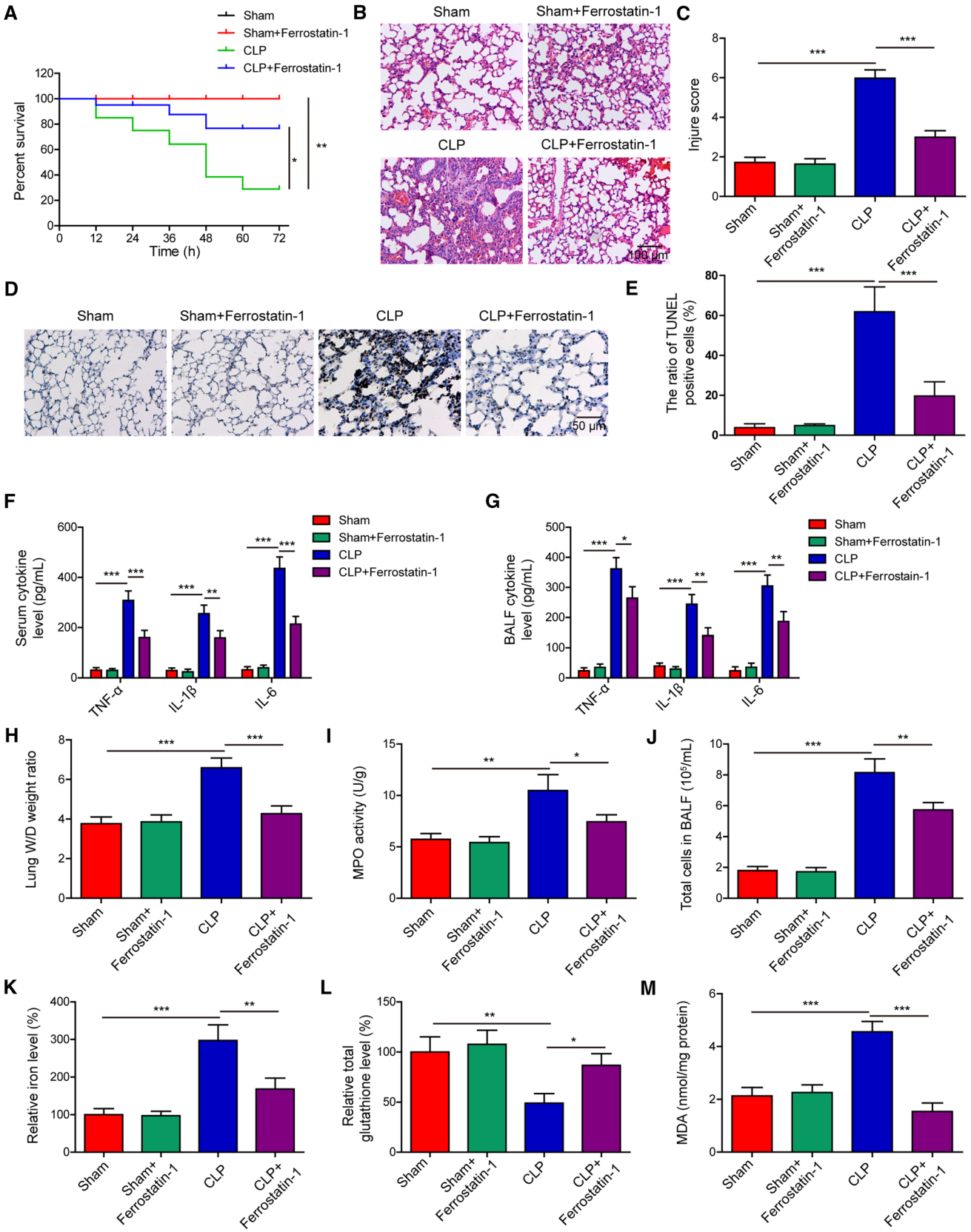
A
Sham
Sham+Ferrostatin-1
CLP
CLP+Ferrostatin-1
Percent survival
Time (h)
B
Sham
Sham+Ferrostatin-1
CLP
CLP+Ferrostatin-1
100 μm
C
Injure score
D
Sham
Sham+Ferrostatin-1
CLP
CLP+Ferrostatin-1
50 μm
E
The ratio of TUNEL positive cells (%)
F
Serum cytokine level (pg/mL)
TNF-α
IL-1β
IL-6
G
BALF cytokine level (pg/mL)
CLP+Ferrostain-1
H
Lung W/D weight ratio
I
MPO activity (U/g)
J
Total cells in BALF (10⁵/mL)
K
Relative iron level (%)
L
Relative total glutathione level (%)
M
MDA (nmol/mg protein)

◂**Fig. 6** Ferroptotic damage mediates sepsis-induced ALI in vivo. Sham- or CLP-operated mice were pre-treated with or without ferrostatin-1 (1 mg/kg body weight, intraperitoneal injection for two consecutive days; $n=20$/group). **A** Percent survival of mice in each group was determined using Kaplan–Meier method. At 24 h after the CLP surgery, **B** representative HE images of lung tissues from each group, scale bar: 100 μm; **C** lung injury was scored and compared between the groups; **D**–**E** cell death in lung tissues examined by TUNEL staining; **F**–**G** the pro-inflammatory cytokines TNF-α, IL-1β, and IL-6 were measured by ELISA from serum **F** and BALF **G** of indicated groups of mice; **H**–**M** lung tissues from indicated groups were measured for lung W/D weight ratio (**H**), MPO activity (**I**), total cells in BALF (**J**), iron (**K**), total glutathione (**L**), and MDA (**M**) levels. $^{*}P<0.05$, $^{**}P<0.01$ and $^{***}P<0.001$

BALF (Fig. 6J), and pulmonary ferroptosis as represented by increased iron (Fig. 6K) and MDA (Fig. 6M) levels, but reduced total glutathione level (Fig. 6L). Together, these in vivo data suggested that inhibiting ferroptosis improved the survival rate of CLP mice, and it significantly alleviated injuries and ferroptotic response in the lung tissues.

AUF1 depletion aggravates CLP-induced lung injuries and ferroptosis

Lastly, we established sepsis-induced ALI model in AUF1 knockout (KO) and wildtype (WT) mice and assessed the effects of AUF1 depletion. The AUF1 KO mice presented no difference in the survival compared with AUF1 WT mice in sham operation group, but the survival rate of AUF1 KO mice was significantly lower than that of WT mice in CLP group (Fig. 7A). In the lung tissues, we observed more severe histological abnormalities (Fig. 7B, C), increased TNF-α, IL-1β and IL-6 levels in serum (Fig. 7D) and BALF (Fig. 7E), increased lung W/D weight ratio (Fig. 7F), pulmonary MPO activity (Fig. 7G), and total cell number in BALF (Fig. 7H) in AUF1 KO mice than in AUF1 WT mice with CLP treatment.

Further analyses of the lung tissues showed that pulmonary iron (Fig. 8A) and MDA (Fig. 8C) levels were significantly elevated in AUF1 WT mice, and were further increased in AUF1 KO mice with CLP operation. In contrast, the pulmonary total glutathione level was significantly reduced in WT mice with CLP operation and was further lowered in AUF1 KO mice (Fig. 8B). On the molecular level, we observed the reduction of GPX4 in CLP-operated WT mice and a further reduction in CLP-operated KO mice (Fig. 8D). In contrast, the expression levels of ASCL4, SLC7A11, and SLC11A2 were significantly increased in CLP-operated WT mice. There were no changes in ASCL4 or SLC11A2 expression between KO and WT mice following CLP operation. But the expression level of SLC7A11 was further induced in KO mice with CLP operation (Fig. 8D-E). Furthermore, we detected significant downregulation of NRF2 and upregulation of ATF3 in lung tissues from KO mice (either in sham-operated or CLP-operated mice, when compared to the corresponding WT mice), on both the protein (Fig. 8F) and the mRNA (Fig. 8G) levels. These findings supported that knocking out AUF1, by down-regulating NRF2 and up-regulating ATF3, promoted ferroptosis in lung tissues and aggravated CLP-induced lung injuries.

Discussion

Several mechanisms responsible for cell death, including apoptosis, oncosis (also known as ischemic cell death) and autophagy, all contribute to ALI [23]. In this study, we demonstrated a new regulatory mechanism of ferroptosis in sepsis-induced ALI. First, ferroptosis could be induced in AECs by different compounds, which was associated with the reduction of AUF1 at both mRNA and protein levels. Second, the E3 ubiquitin ligase FBXW7 mediated the ubiquitination of AUF1 through the proteasome pathway, thereby promoting the degradation of AUF1 protein during ferroptosis. Third, AUF1 played a vital role in inhibiting ferroptosis by regulating NRF2 and ATF3 inversely. Fourth, the depletion of AUF1 shortened the survival rate and increased the lung injuries of septic mice, which was associated with aggravated ferroptosis.

Ferroptosis is a cell death distinct from apoptosis and characterized by iron-dependent accumulation of lipid peroxides [8, 9, 24]. Since the concept of ferroptosis was first proposed in 2012 [25], increasing information has been acquired on its mechanism and significance in multiple organs and disease paradigms, such as cancers [26–28], renal failure [29–31], and heart failure [32, 33]. Sepsis is an infection-induced clinical condition that often rapidly progresses into multiple organ dysfunction syndrome as a result of complicated interaction involving multiple cell types, tissues, organs, and systems [34]. Over the past few years, evidence has begun to suggest a link between ferroptosis and sepsis. GPX4, the essential negative regulator for ferroptosis by targeting lipid peroxidation, inhibited macrophage pyroptosis and alleviated polymicrobial septic lethality [35]. Dexmedetomidine, by targeting myocardial ferroptosis, rescued septic heart injury [36]. In this study, using an in vivo sepsis-induced ALI model, we showed that inhibition of ferroptosis with ferrostatin-1 significantly alleviated ALI symptoms and pulmonary ferroptosis, supporting the involvement of ferroptosis in at least sepsis-induced ALI. We also noticed not only the benefits of ferrostatin-1 produced in the lung tissues, but also its significant effects on improving the survival and inhibiting inflammation response, suggesting that ferroptosis may act on multiple tissues, organs, or systems, and present diverse biological effects. For example, Erastin, a ferroptosis-inducer, inhibited

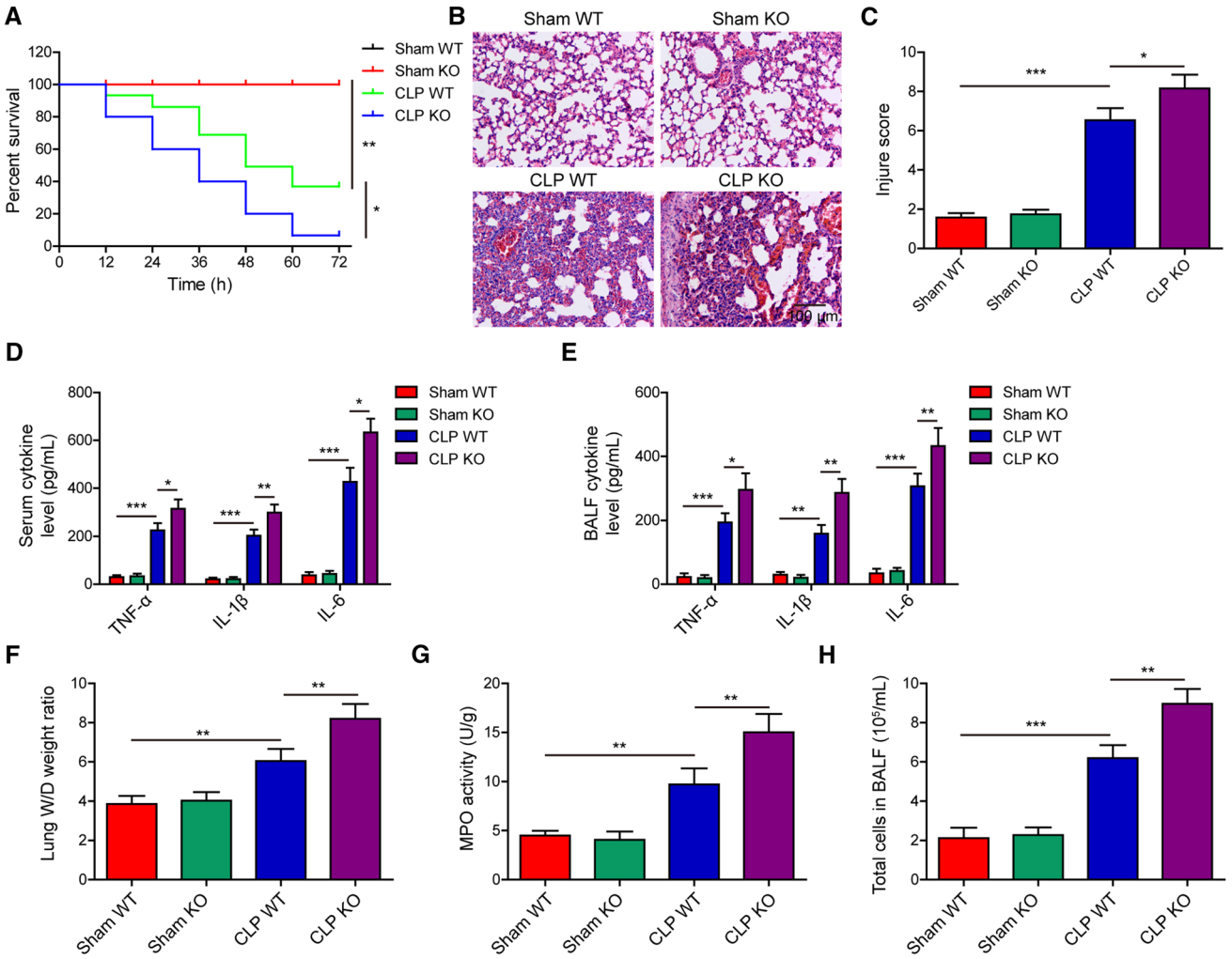

Fig. 7 AUF1 depletion aggravates CLP-induced lung injuries. Sham or CLP operation was performed in AUF1 wildtype (WT) or knockout (KO) mice (n = 20/group). **A** Percent survival of mice in each group was determined using Kaplan–Meier method. At 24 h after the surgery, **B** representative HE images of lung tissues from each group, scale bar: 100 μm; **C** lung injury was scored and compared between the indicated groups; **D**–**E** the pro-inflammatory cytokines TNF-α, IL-1β, and IL-6 were measured by ELISA from serum **D** and BALF **E** of indicated groups of mice; **F**–**H** lung tissues from indicated groups were measured for lung W/D weight ratio (**F**), MPO activity (**G**), and total cells in BALF (**H**). $^{*}P < 0.05$, $^{**}P < 0.01$ and $^{***}P < 0.001$

the NF-κB signaling pathway and the expression of inflammatory cytokines (such as TNF-α and IL-1β) in lipopolysaccharide-challenged macrophages and alleviated septic shock [37]. In contrast, NF-κB signaling was shown to target ferroptosis in ER stress-challenged intestinal epithelial cells and to alleviate ulcerative colitis [38]. Therefore, future studies should focus on the differential mechanisms and effects of ferroptosis under different conditions of sepsis in order to develop specific strategies to maintain the benefits and limit the side effects of ferroptosis. In the in vivo model used in this study, we administered ferrostatin-1 for 48 h before CLP procedure, which, although demonstrated the important contribution of ferroptosis in ALI development, is not quite practical in clinical settings. Consequently, it would be interesting to examine in the future study whether a similar protective effect would be achieved if ferrostatin-1 is administered after CLP.

In addition to revealing the importance of ferroptosis in sepsis-induced ALI, we identified AUF1 as a new important player in ferroptosis. Besides its well characterized function as an ARE-binding protein that regulates mRNA degradation on the post-transcriptional level as well as gene expression on transcriptional or translational level, AUF1 plays diverse roles in multiple physiological and pathological paradigms [39]. In this study, we showed for the first time that AUF1 was down-regulated in AECs challenged with multiple ferroptosis-inducing compounds, both on the mRNA and protein levels, suggesting the functional importance of reducing AUF1 in executing ferroptosis in these cells. Consistently, the overexpression of AUF1 in Erastin-challenged

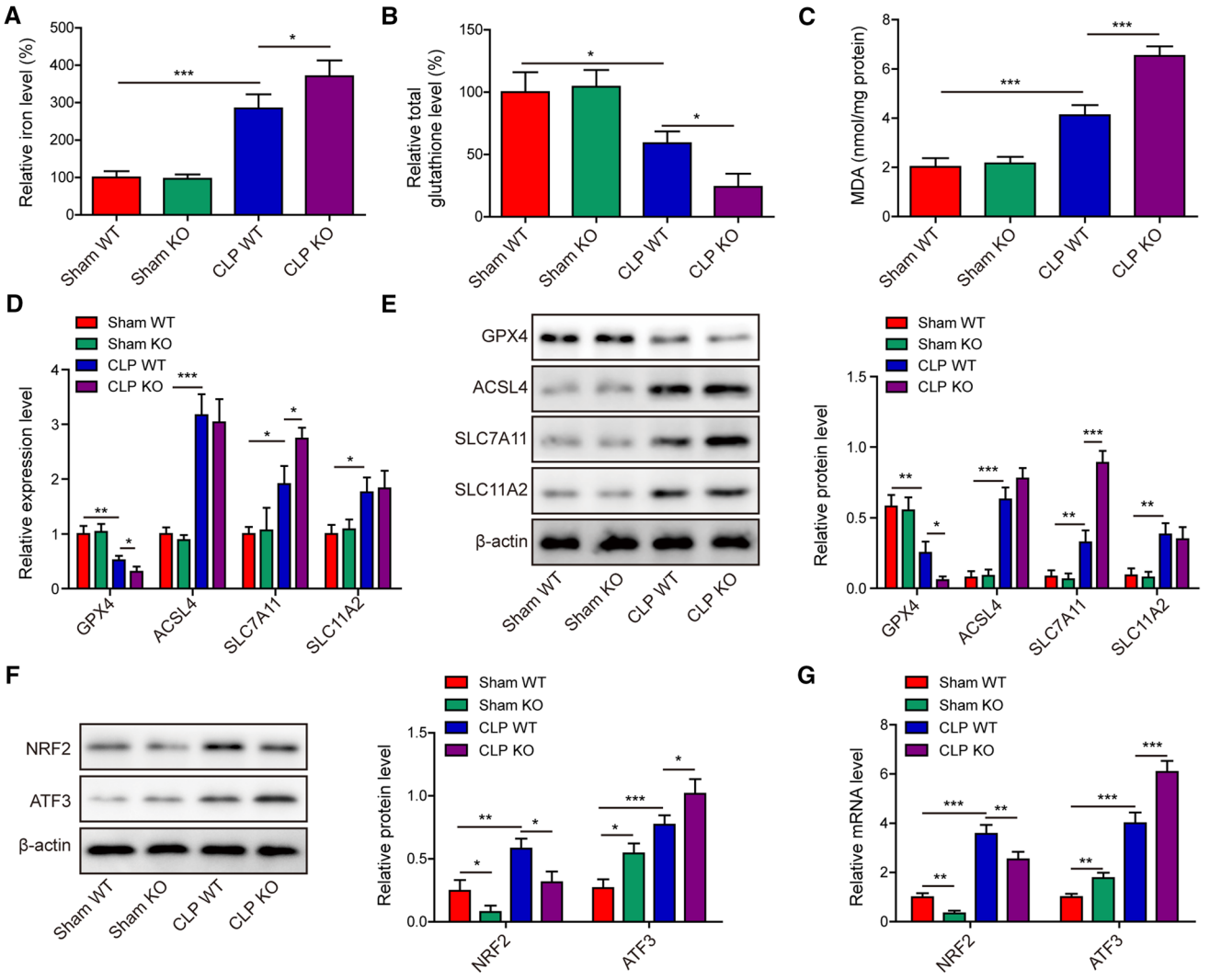

Fig. 8 AUF1 depletion exacerbates CLP-induced ferroptosis in lung tissues. Sham or CLP operation was performed in AUF1 wildtype (WT) or knockout (KO) mice ($n=20$/group). At 24 h after the surgery, **A**–**C** lung tissues from indicated groups were measured for iron (**A**), total glutathione (**B**), and MDA (**C**) levels; **D**–**E** the expression levels of GPX4, ACSL4, SLC7A11 and SLC11A2 in lung tissues by RT-PCR **D** and western blot (**E**); **F**–**G** the expression levels of NRF2 and ATF3 in lung tissues were tested by western blot **F** and RT-PCR (**G**). $^{*}P<0.05$, $^{**}P<0.01$ and $^{***}P<0.001$

AECs was sufficient to reverse all ferroptotic phenotypes. In the sepsis-induced ALI model, we showed that the survival rate of AUF1 KO mice was significantly lower than that of WT mice. Correspondingly, lung injury and pulmonary ferroptosis were more severe in CLP-operated AUF1 KO mice, supporting the essential role of AUF1 in antagonizing ferroptosis and sepsis-induced ALI. Similar to our findings, Lu et al. showed that endotoxic shock was more severe in AUF1 KO mice and was associated with the failure to degrade the mRNAs of pro-inflammatory cytokines, such as TNF-α and IL-1β [11].

The functional diversity of AUF1 is partly contributed by four different AUF1 isoforms that reside in different subcellular compartments or by the crosstalk between AUF1 and other mRNA-binding proteins. For example, HuR and AUF1 frequently co-occupy and co-regulate (synergistically, sequentially, or oppositely) the same mRNA target [40–42]. Although we did not analyze the mechanism leading to reduced AUF1 mRNA or characterize the AUF1 isoforms in AECs, we did identify the E3 ubiquitin ligase FBXW7, which is responsible for the degradation of AUF1 protein in ferroptotic AECs. Zhang et al. reported that FBXW7 contributed to ferroptosis by targeting ZEP36 protein expression [43]. We further showed that AUF1 stabilized the stability of NRF2 mRNA and at the same time promoted the degradation of ATF3 mRNA, and both were functionally important for AUF1-mediated resistance to ferroptosis. Consistent with our

findings, Poganik et al. reported that by binding to the 3'-UTR of NRF2 mRNA, HuR promoted the NRF2 mRNA maturation and nuclear export, and AUF1 stabilized NRF2 mRNA, thus collectively enhancing NRF2 activity [13]. Pan et al. showed that HuR and AUF1 oppositely regulated ATF3 mRNA stability [12]. Although we are not clear about the mechanisms underlying the differential regulation of NRF2 and ATF3 by AUF1 in ferroptotic AECs, we did notice that AUF1 bound not just to CDS and 3'-UTR of NRF2 mRNA, but it also bound to the 3'-UTR of ATF3 mRNA. Furthermore, unlike AUF1, HuR was up-regulated in Erastin-treated AECs, suggesting their opposite expressions and crosstalk may also contribute to ferroptosis.

The role and significance of NRF2 in ferroptosis have been quite well established [21]. As a transcription factor, NRF2 regulated multiple genes constituting ferroptotic cascade, including but not limited to GPX4, SLC7A11, HO-1, the glutamate cysteine ligase, ferroportin, and ferritin [21, 44]. As a result, targeting NRF2 to alter ferroptosis has proved beneficial for certain diseases, such as neurodegeneration and cancers [45–49]. In our study, we showed the inhibitor of ferroptosis, Liproxstatin-1, reversed the ferroptosis-promoting effects in AECs caused by NRF2 silence. In contrast, the role of ATF3 in ferroptosis is still poorly understood. Wang et al. showed that ATF3 negatively regulated the transcription of SLC7A11 and promoted ferroptosis [10]. In this study, we showed that AUF1 was sufficient to up-regulate both GPX4 and SLC7A11, but not the other two ferroptosis-related markers ACSL4 and SLC11A2 in Erastin-treated AECs. Furthermore, the regulation on GPX4 was achieved by up-regulating NRF2, while the upregulation of SLC7A11 was obtained by down-regulating ATF3, although another study suggested that NRF2 could regulate the expression of SLC7A11 [50]. At this point, although it is not clear whether Erastin directly regulates the transcription of GPX4, downregulating the AUF1/NRF2 pathway is a potential mechanism by which Erastin downregulates GPX4 in AECs.

In summary, we demonstrated the pivotal role of AUF1, by oppositely regulating two transcription factors, NRF2 and ATF3, in protecting AECs against ferroptosis. This anti-ferroptotic role of AUF1 alleviated sepsis-induced ALI and prolonged sepsis-induced survival. Thus, boosting AUF1 signaling may be beneficial in the treatment of sepsis-induced ALI. Since the study was only performed in cultured cells and sepsis-induced ALI mice, we should carefully examine the relevance of current findings to clinical condition in future studies. Also, exploration AUF1 signaling in the regulation of ferroptosis under treatment of other ferroptosis-inducing compounds such as sorafenib, Sulfasalazine, and RSL3 also will strengthen our conclusion.

Supplementary Information The online version contains supplementary material available at https://doi.org/10.1007/s00018-022-04248-8.

Acknowledgements We would like to give our sincere gratitude to the reviewers for their constructive comments.

Authors' contribution Guarantor of integrity of the entire study: CD, WYC. Study concepts: WYC, TDL. Study design: WYC, TDL, SXF. Definition of intellectual content: WYC, SXF. Literature research: XH, GFF, PF. Experimental studies: GFF, WYC, CDY. Data acquisition: JMW, GFF. Data analysis: XH, SXF. Statistical analysis: JMW, XH. Manuscript preparation: XH, CDY. Manuscript editing: SXF. Manuscript review: WYC, TDL. All authors read and approved the final manuscript.

Funding This work was supported by National Natural Science Foundation of China (No.31872800), Foundation of The Third Affiliated Hospital of Guangzhou Medical University (No.2019Z02) and Foundation of Guangzhou Science and Technology Burea (No.202102010089).

Availability of data and materials All data generated or analyzed during this study are included in this published article.

Declarations

Ethical approval All animal protocols were reviewed and approved by the Institutional Animal Care and Use Committee of Guangzhou Medical University (Guangzhou, Guangdong, China).

Informed consent The informed consent obtained from study participants.

Conflict of interest The authors declare that they have no conflict of interest.

References

1. Vincent JL, Zambon M (2006) Why do patients who have acute lung injury/acute respiratory distress syndrome die from multiple organ dysfunction syndrome? Implications for management. Clin Chest Med 27:725–731. https://doi.org/10.1016/j.ccm.2006.06.010
2. Johnson ER, Matthay MA (2010) Acute lung injury: epidemiology, pathogenesis, and treatment. J Aerosol Med Pulm Drug Deliv 23:243–252. https://doi.org/10.1089/jamp.2009.0775
3. Mokra D, Kosutova P (2015) Biomarkers in acute lung injury. Respir Physiol Neurobiol 209:52–58. https://doi.org/10.1016/j.resp.2014.10.006
4. Li X, Zhuang X, Qiao T (2019) Role of ferroptosis in the process of acute radiation-induced lung injury in mice. Biochem Biophys Res Commun 519:240–245. https://doi.org/10.1016/j.bbrc.2019.08.165
5. Li Y et al (2020) Inhibitor of apoptosis-stimulating protein of p53 inhibits ferroptosis and alleviates intestinal ischemia/reperfusion-induced acute lung injury. Cell Death Differ. https://doi.org/10.1038/s41418-020-0528-x
6. Liu P et al (2020) Ferrostatin-1 alleviates lipopolysaccharide-induced acute lung injury via inhibiting ferroptosis. Cell Mol Biol Lett 25:10. https://doi.org/10.1186/s11658-020-00205-0

7. Zhou H et al (2019) Ferroptosis was involved in the oleic acid-induced acute lung injury in mice. Sheng Li Xue Bao 71:689–697
8. Li J et al (2020) Ferroptosis: past, present and future. Cell Death Dis 11:88. https://doi.org/10.1038/s41419-020-2298-2
9. Xie Y et al (2016) Ferroptosis: process and function. Cell Death Differ 23:369–379. https://doi.org/10.1038/cdd.2015.158
10. Wang L et al (2020) ATF3 promotes erastin-induced ferroptosis by suppressing system Xc(). Cell Death Differ 27:662–675. https://doi.org/10.1038/s41418-019-0380-z
11. Lu JY, Sadri N, Schneider RJ (2006) Endotoxic shock in AUF1 knockout mice mediated by failure to degrade proinflammatory cytokine mRNAs. Genes Dev 20:3174–3184. https://doi.org/10.1101/gad.1467606
12. Pan YX, Chen H, Kilberg MS (2005) Interaction of RNA-binding proteins HuR and AUF1 with the human ATF3 mRNA 3'-untranslated region regulates its amino acid limitation-induced stabilization. J Biol Chem 280:34609–34616. https://doi.org/10.1074/jbc.M507802200
13. Poganik JR et al (2019) Post-transcriptional regulation of Nrf2-mRNA by the mRNA-binding proteins HuR and AUF1. FASEB J 33:14636–14652. https://doi.org/10.1096/fj.201901930R
14. Martinez AM, Kim A, Yang WS (2020) Detection of Ferroptosis by BODIPY 581/591 C11. Methods Mol Biol 2108:125–130. https://doi.org/10.1007/978-1-0716-0247-8_11
15. Rittirsch D, Huber-Lang MS, Flierl MA, Ward PA (2009) Immunodesign of experimental sepsis by cecal ligation and puncture. Nat Protoc 4:31–36. https://doi.org/10.1038/nprot.2008.214
16. Li XH et al (2013) Protective effects of polydatin on septic lung injury in mice via upregulation of HO-1. Mediators Inflamm 2013:354087. https://doi.org/10.1155/2013/354087
17. Han H, Ziegler SF (2013) Bronchoalveolar lavage and lung tissue digestion. Bio Protoc. https://doi.org/10.21769/bioprotoc.859
18. Laroia G, Cuesta R, Brewer G, Schneider RJ (1999) Control of mRNA decay by heat shock-ubiquitin-proteasome pathway. Science 284:499–502. https://doi.org/10.1126/science.284.5413.499
19. Fan BY et al (2021) Liproxstatin-1 is an effective inhibitor of oligodendrocyte ferroptosis induced by inhibition of glutathione peroxidase 4. Neural Regen Res 16:561–566. https://doi.org/10.4103/1673-5374.293157
20. Miotto G et al (2020) Insight into the mechanism of ferroptosis inhibition by ferrostatin-1. Redox Biol 28:101328. https://doi.org/10.1016/j.redox.2019.101328
21. Dodson M, Castro-Portuguez R, Zhang DD (2019) NRF2 plays a critical role in mitigating lipid peroxidation and ferroptosis. Redox Biol 23:101107. https://doi.org/10.1016/j.redox.2019.101107
22. Zhu H, Santo A, Jia Z, Robert Li Y (2019) GPx4 in bacterial infection and polymicrobial sepsis: involvement of ferroptosis and pyroptosis. React Oxyg Species (Apex) 7:154–160. https://doi.org/10.20455/ros.2019.835
23. Tang PS, Mura M, Seth R, Liu M (2008) Acute lung injury and cell death: how many ways can cells die? Am J Physiol Lung Cell Mol Physiol 294:L632-641. https://doi.org/10.1152/ajplung.00262.2007
24. Lei P, Bai T, Sun Y (2019) Mechanisms of ferroptosis and relations with regulated cell death: a review. Front Physiol 10:139. https://doi.org/10.3389/fphys.2019.00139
25. Dixon SJ et al (2012) Ferroptosis: an iron-dependent form of nonapoptotic cell death. Cell 149:1060–1072. https://doi.org/10.1016/j.cell.2012.03.042
26. Friedmann Angeli JP, Krysko DV, Conrad M (2019) Ferroptosis at the crossroads of cancer-acquired drug resistance and immune evasion. Nat Rev Cancer 19:405–414. https://doi.org/10.1038/s41568-019-0149-1
27. Hassannia B, Vandenabeele P, Vanden Berghe T (2019) Targeting Ferroptosis to Iron Out Cancer. Cancer Cell 35:830–849. https://doi.org/10.1016/j.ccell.2019.04.002
28. Mou Y et al (2019) Ferroptosis, a new form of cell death: opportunities and challenges in cancer. J Hematol Oncol 12:34. https://doi.org/10.1186/s13045-019-0720-y
29. Friedmann Angeli JP et al (2014) Inactivation of the ferroptosis regulator Gpx4 triggers acute renal failure in mice. Nat Cell Biol 16:1180–1191. https://doi.org/10.1038/ncb3064
30. Linkermann A et al (2014) Synchronized renal tubular cell death involves ferroptosis. Proc Natl Acad Sci U S A 111:16836–16841. https://doi.org/10.1073/pnas.1415518111
31. Muller T et al (2017) Necroptosis and ferroptosis are alternative cell death pathways that operate in acute kidney failure. Cell Mol Life Sci 74:3631–3645. https://doi.org/10.1007/s00018-017-2547-4
32. Chen X, Xu S, Zhao C, Liu B (2019) Role of TLR4/NADPH oxidase 4 pathway in promoting cell death through autophagy and ferroptosis during heart failure. Biochem Biophys Res Commun 516:37–43. https://doi.org/10.1016/j.bbrc.2019.06.015
33. Liu B et al (2018) Puerarin protects against heart failure induced by pressure overload through mitigation of ferroptosis. Biochem Biophys Res Commun 497:233–240. https://doi.org/10.1016/j.bbrc.2018.02.061
34. Rossaint J, Zarbock A (2015) Pathogenesis of multiple organ failure in sepsis. Crit Rev Immunol 35:277–291. https://doi.org/10.1615/critrevimmunol.2015015461
35. Kang R et al (2018) Lipid peroxidation drives gasdermin D-mediated pyroptosis in lethal polymicrobial sepsis. Cell Host Microbe 24:97-108.e104. https://doi.org/10.1016/j.chom.2018.05.009
36. Wang C et al (2020) Dexmedetomidine alleviated sepsisinduced myocardial ferroptosis and septic heart injury. Mol Med Rep 22:175–184. https://doi.org/10.3892/mmr.2020.11114
37. Oh BM et al (2019) Erastin inhibits septic shock and inflammatory gene expression via suppression of the NF-kappaB pathway. J Clin Med. https://doi.org/10.3390/jcm8122210
38. Xu M et al (2020) Ferroptosis involves in intestinal epithelial cell death in ulcerative colitis. Cell Death Dis 11:86. https://doi.org/10.1038/s41419-020-2299-1
39. Moore AE, Chenette DM, Larkin LC, Schneider RJ (2014) Physiological networks and disease functions of RNA-binding protein AUF1. Wiley Interdiscip Rev RNA 5:549–564. https://doi.org/10.1002/wrna.1230
40. Barker A et al (2012) Sequence requirements for RNA binding by HuR and AUF1. J Biochem 151:423–437. https://doi.org/10.1093/jb/mvs010
41. Lal A et al (2004) Concurrent versus individual binding of HuR and AUF1 to common labile target mRNAs. EMBO J 23:3092–3102. https://doi.org/10.1038/sj.emboj.7600305
42. Trojanowicz B, Dralle H, Hoang-Vu C (2011) AUF1 and HuR: possible implications of mRNA stability in thyroid function and disorders. Thyroid Res. https://doi.org/10.1186/1756-6614-4-S1-S5
43. Zhang Z et al (2019) RNA-binding protein ZFP36/TTP protects against ferroptosis by regulating autophagy signaling pathway in hepatic stellate cells. Autophagy. https://doi.org/10.1080/15548627.2019.1687985
44. Kerins MJ, Ooi A (2018) The Roles of NRF2 in Modulating Cellular Iron Homeostasis. Antioxid Redox Signal 29:1756–1773. https://doi.org/10.1089/ars.2017.7176
45. Abdalkader M, Lampinen R, Kanninen KM, Malm TM, Liddell JR (2018) Targeting Nrf2 to Suppress Ferroptosis and

Mitochondrial Dysfunction in Neurodegeneration. Front Neurosci 12:466. https://doi.org/10.3389/fnins.2018.00466
46. Huang HX et al (2020) TFAP2A is a novel regulator that modulates ferroptosis in gallbladder carcinoma cells via the Nrf2 signalling axis. Eur Rev Med Pharmacol Sci 24:4745–4755. https://doi.org/10.26355/eurrev_202005_21163
47. Liu Q, Wang K (2019) The induction of ferroptosis by impairing STAT3/Nrf2/GPx4 signaling enhances the sensitivity of osteosarcoma cells to cisplatin. Cell Biol Int 43:1245–1256. https://doi.org/10.1002/cbin.11121
48. Roh JL, Kim EH, Jang H, Shin D (2017) Nrf2 inhibition reverses the resistance of cisplatin-resistant head and neck cancer cells to artesunate-induced ferroptosis. Redox Biol 11:254–262. https://doi.org/10.1016/j.redox.2016.12.010
49. Song X, Long D (2020) Nrf2 and ferroptosis: a new research direction for neurodegenerative diseases. Front Neurosci 14:267. https://doi.org/10.3389/fnins.2020.00267
50. Shin CS et al (2017) The glutamate/cystine xCT antiporter antagonizes glutamine metabolism and reduces nutrient flexibility. Nat Commun 8:15074. https://doi.org/10.1038/ncomms15074